Molecular Physics

An International Journal at the Interface Between Chemistry and Physics

ISSN: 0026-8976 (Print) 1362-3028 (Online) Journal homepage: http://www.tandfonline.com/loi/tmph20

Full-dimensional simulation of the laser-induced alignment dynamics of H_2He^+

Tamás Szidarovszky & Kaoru Yamanouchi

To cite this article: Tamás Szidarovszky & Kaoru Yamanouchi (2017): Full-dimensional simulation of the laser-induced alignment dynamics of H_2He^+, Molecular Physics

To link to this article: http://dx.doi.org/10.1080/00268976.2017.1297863

Published online: 20 Mar 2017.

MOLECULAR PHYSICS, 2017
https://doi.org/10.1080/00268976.2017.1297863

Taylor & Francis
Taylor & Francis Group

BANDRAUK

Full-dimensional simulation of the laser-induced alignment dynamics of H_2He^+

Tamás Szidarovszky and Kaoru Yamanouchi

Department of Chemistry, School of Science, The University of Tokyo, Tokyo, Japan

ABSTRACT

A theoretical approach for simulating the laser-induced alignment dynamics of non-rigid polyatomic molecules is introduced, in which the time-dependent Schrödinger equation (TDSE) is solved by expanding the laser-induced wavepacket with the field-free rovibrational eigenstates of the system. It is shown that not only the exact solution of the TDSE but also its approximated solution can be obtained, depending on the choices of the method for determining the field-free eigenstates. Laser-induced alignment of weakly bound H_2He^+ is investigated by adopting the present approach with high-accuracy full-dimensional variational calculations of the nuclear dynamics.

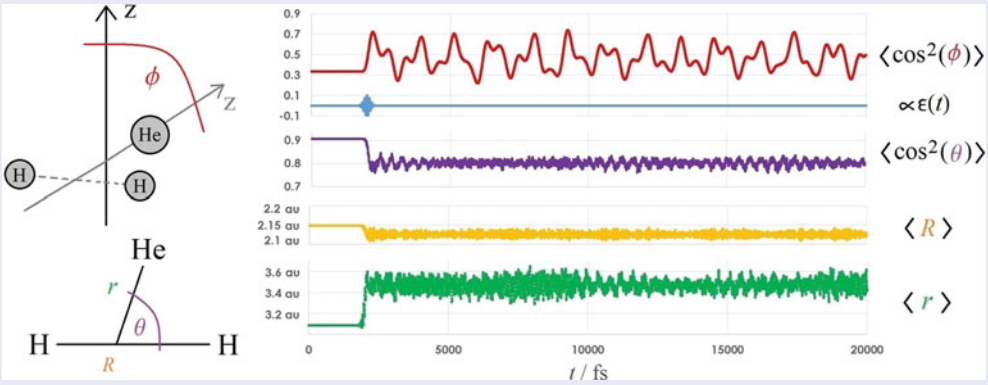

ARTICLE HISTORY
Received 25 November 2016
Accepted 10 February 2017

KEYWORDS
H_2He^+; molecular alignment; intense laser physics; rovibrational wavepacket; variational nuclear motion computation

1. Introduction

Recent developments of laser technology enabled researchers to align molecules in a space by ultrashort laser pulses, and, in these decades, a variety of studies have been reported on alignment of molecules. The mechanism of the alignment process has also been investigated theoretically and the experimental results have been interpreted successfully by numerical simulations [1–5].

In most of these previous theoretical studies, molecules have been treated as rigid or semi-rigid molecules whose geometrical structure does not change largely in the course of the alignment, and simulations beyond the rigid rotor model and its perturbative corrections have been made for only several cases. For example, the effect of the torsional motion was examined in the aligment of B_2F_4 [6], and the simultaneous interactions of the dipole moment and the polarisability with the external field was studied in the alignment processes of HCN [7]. The effects of rovibrational coupling during the alignment was also investigated for HF [8].

However, in the case of floppy molecules having one or more large-amplitude vibrational modes with the strong rovibrational couplings, the rigid rotor approximation and its perturbative extensions could not describe properly the alignment processes [9], because the rovibrational couplings could lead to substantial variation of the rotational constants in the course of the alignment.

In order to describe simultaneously the rovibrational motion and alignment of such floppy molecules, it becomes necessary to introcude non-perturbative approaches, in which variational wavefunction expansions, accurate potential energy surfaces, and exact kinetic energy operators are emlpoyed [10,11]. However, it has been known that performing such non-perturbative theoretical simulations of the rovibrational motion of polyatomic molecules is a demanding task even

CONTACT Tamás Szidarovszky tamas821@gmail.com; Kaoru Yamanouchi kaoru@chem.s.u-tokyo.ac.jp

under field-free conditions [10,11]. This becomes even more difficult in the presence of an external field due to the field-induced couplings among rovibrational levels. Therefore, it would be a challenge to describe the spatial alignment of such floppy molecules with high accuracy by performing numerical simulations of their rovibrational excitation.

In the present study, we propose a theoretical framework of describing accurately the laser-induced rovibrational motion and spatial alignment of non-rigid polyatomic molecules and its implementation into full-dimensional as well as reduced-dimensional variational computations by taking advantage of the efficient computational methods of nuclear dynamics developed in the past two decades [10,12,13], and we demonstrate the applicability of the present approach by numerical simulations of the alignment dynamics of a weakly bound and floppy complex molecule of $[H_2–He]^+$ induced by an ultrashort laser pulse.

2. Theoretical methods

2.1. Laser-induced rovibrational dynamics

In order to simulate spatial alignment dynamics of molecules, one needs to solve the time-dependent Schrödinger equation (TDSE)

$$i\hbar\frac{\partial\left|\Psi\left(t\right)\right\rangle}{\partial t}=\hat{H}\left(t\right)\left|\Psi\left(t\right)\right\rangle,$$
$$\hat{H}\left(t\right)=\hat{H}_0-\boldsymbol{\varepsilon}\left(t\right)\boldsymbol{\mu}-\frac{1}{2}\boldsymbol{\varepsilon}\left(t\right)\left(\boldsymbol{\alpha}\boldsymbol{\varepsilon}\left(t\right)\right), \quad (1)$$

where $\hat{H}_0$, $-\boldsymbol{\varepsilon}(t)\boldsymbol{\mu}$ and $-(1/2)\boldsymbol{\varepsilon}(t)(\boldsymbol{\alpha}\boldsymbol{\varepsilon}(t))$ are the field-free rovibrational Hamiltonian, the permanent dipole interaction with the external field $\boldsymbol{\varepsilon}(t)$ and the induced dipole interaction with the external field $\boldsymbol{\varepsilon}(t)$, respectively.

We propose here a two-step approach for solving Equation (1). The first step is to determine bound rovibrational states $|\Psi_n\rangle$, satisfying the time-independent nuclear Schrödinger equation

$$\hat{H}_0\left|\Psi_n\right\rangle=E_n\left|\Psi_n,\right\rangle \quad (2)$$

leading to a small set of basis functions describing the rovibrational motion of the system. In the second step, the time-dependent rovibrational wavepacket $|\Psi(t)\rangle$ is expanded in terms of $|\Psi_n\rangle$, leading to a compact matrix representation of the Hamiltonian, with which time propagation can be carried out in a straightforward manner.

Naturally, the accuracy and approximations made to solve the time-independent Schrödinger equation (Equation (2)) will limit the accuracy of the time-dependent calculations. In the case of triatomic molecules, full-dimensional, variational rovibrational calculations can in principle be carried out to derive all their bound rovibrational states (see e.g. [14]), leading to a complete and numerically exact basis set to represent the laser-induced time-dependent rovibrational dynamics. Although relevant methods and computer softwares are available [10,12,13] for treating accurately larger molecular systems having four or more atoms, such calculations are in general very demanding. Nonetheless, variational reduced-dimensional approaches [15] can be utilised, in which only selected degrees of freedom that are most relevant for describing the laser-induced dynamics of the molecule are taken into account. Additionally, approximations commonly adopted in theoretical molecular spectroscopy such as the harmonic oscillator approximation and its perturbative extensions [9,16] can be introduced for solving Equation (2). In most of the computer codes that have been developed for solving Equation (2), the full- or reduced-dimensional rovibrational wavefunctions of a field-free molecular system are generated by expanding the nuclear wave function as

$$\left|\Psi_n\right\rangle\equiv\left|\Psi^{JMn}\right\rangle=\sum_{K,v}C_{Kv}^{Jn}\left|v\right\rangle\left|JKM\right\rangle, \quad (3)$$

where C_{Kv}^{Jn} is an expansion coefficient, $|v\rangle$ is the vth vibrational basis function, $|JKM\rangle$ is a symmetric-top eigenfunction [17], J is the rotational quantum number, M is the projection of rotational angular momentum onto the space fixed z-axis, K is the projection of rotational angular momentum onto the body-fixed (BF) z-axis, n is 'all other' quantum numbers. In coordinate representation, the rovibrational wavefunctions might be written as

$$\Psi^{JMn}\left(Q_1,\ldots,Q_d,\varphi,\vartheta,\chi\right)$$
$$=\sqrt{\frac{2J+1}{8\pi^2}}\sum_{K,v}C_{Kv}^{Jn}\psi_v\left(Q_1,\ldots,Q_d\right)D_{MK}^{J\ *}\left(\varphi,\vartheta,\chi\right), \quad (4)$$

where $\psi_v(Q_1,\ldots,Q_d)$ is the vth vibrational basis function describing d vibrational degrees of freedom and $D_{MK}^{J}(\varphi,\vartheta,\chi)$ is a Wigner matrix [17] represented using the three Euler angles, φ, ϑ and χ, describing the orientation of the BF coordinate frame with respect to the laboratory-fixed (LF) frame.

In the present study, we construct the matrix representation of the Hamiltonian of Equation (1) using

the basis of field-free states $|\Psi^{JMn}\rangle$. Because the expression for the external field $\boldsymbol{\varepsilon}(t)$ in Equation (1) is given in the LF frame, the molecular properties $\boldsymbol{\mu}$ and $\boldsymbol{\alpha}$, which are obtained by quantum chemistry calculations in a BF coordinate frame, need to be expressed in the LF frame. A convenient approach is to change the Cartesian representation to the so-called spherical basis [17] representation using the transformation formulae $\mu^{(1,0)} = \mu_3$, $\mu^{(1,\pm1)} = \frac{1}{\sqrt{2}}(\mp\mu_1 - i\mu_2)$, $\alpha^{(0)} = -\frac{1}{\sqrt{3}}(\alpha_{11}+\alpha_{22}+\alpha_{33}) = -\frac{1}{\sqrt{3}}\mathrm{Tr}[\boldsymbol{\alpha}]$, $\alpha^{(2,\pm2)} = \frac{1}{2}[\alpha_{11}-\alpha_{22} \pm i(\alpha_{12}+\alpha_{21})]$, $\alpha^{(2,\pm1)} = \frac{1}{2}[\mp(\alpha_{13}+\alpha_{31}) - i(\alpha_{23}+\alpha_{32})]$ and $\alpha^{(2,0)} = \frac{1}{\sqrt{6}}[2\alpha_{33}-\alpha_{22}-\alpha_{11}]$. In the spherical basis representation, the rotation between the BF coordinate frame and LF coordinate frame can be performed by multiplying with the Wigner matrices, i.e. the jth component of a spherical tensor of rank l in the LF frame $T^{\mathrm{LF},(l,j)}$ is transformed into its BF components $T^{\mathrm{BF},(l,j)}$ as [17]

$$T^{\mathrm{LF},(l,j)} = \sum_{k=-l}^{l} D^{l}_{jk}{}^{*}(\varphi,\vartheta,\chi)\, T^{\mathrm{BF},(l,k)}. \tag{5}$$

Assuming a linearly polarised external field $\boldsymbol{\varepsilon}^{\mathrm{LF}} = (0,0,\varepsilon)$, the interaction terms in Equation (1) can be written using Equation (5) as

$$\begin{aligned}
\boldsymbol{\varepsilon}^{\mathrm{LF}}\boldsymbol{\mu}^{\mathrm{LF}} &= \varepsilon\mu^{\mathrm{LF}}_3 = \varepsilon\mu^{\mathrm{LF},(1,0)} = \varepsilon\sum_{k=-1}^{1} D^{1}_{0k}{}^{*}(\varphi,\vartheta,\chi)\mu^{\mathrm{BF},(1,k)}\\
\boldsymbol{\varepsilon}^{\mathrm{LF}}\left(\boldsymbol{\alpha}^{\mathrm{LF}}\boldsymbol{\varepsilon}^{\mathrm{LF}}\right) &= \varepsilon^2\alpha^{\mathrm{LF}}_{33} =\\
&= \varepsilon^2\frac{\sqrt{6}}{3}\left(\alpha^{\mathrm{LF},(2,0)} - \frac{1}{\sqrt{2}}\alpha^{\mathrm{LF},(0)}\right)\\
&= \varepsilon^2\frac{\sqrt{6}}{3}\left[\sum_{k=-2}^{2} D^{2}_{0k}{}^{*}(\varphi,\vartheta,\chi)\,\alpha^{\mathrm{BF},(2,k)}\right.\\
&\quad\left. - \frac{1}{\sqrt{2}}\alpha^{\mathrm{BF},(0)}\right].
\end{aligned}$$

Based on the wavefunction expansions of Equations (3) and (4) and the integral formula of the Wigner matrices represented by 3j-symbols [17],

$$\begin{aligned}
&\int D^{J_1}_{M_1'M_1}(R)\, D^{J_2}_{M_2'M_2}(R)\, D^{J_3}_{M_3'M_3}(R)\, dR\\
&\quad = 8\pi^2\begin{pmatrix} J_1 & J_2 & J_3\\ M_1' & M_2' & M_3'\end{pmatrix}\begin{pmatrix} J_1 & J_2 & J_3\\ M_1 & M_2 & M_3\end{pmatrix},
\end{aligned} \tag{6}$$

where R represents an operation in the SO(3) rotation group, the matrix elements of the Hamiltonian of Equation (1) can be expressed as

$$\begin{aligned}
&\left\langle\Psi^{JMn}\left|\widehat{H}\right|\Psi^{J'M'n'}\right\rangle\\
&= E^{Jn}\delta_{JJ'}\delta_{nn'}\delta_{MM'} - \varepsilon(t)\sum_{k=-1}^{1}\left\langle\Psi^{JMn}\left|D^{1}_{0k}{}^{*}\mu^{\mathrm{BF},(1,k)}\right|\Psi^{J'M'n'}\right\rangle\\
&\quad - \frac{\varepsilon(t)^2}{\sqrt{6}}\left[\sum_{k=-2}^{2}\left\langle\Psi^{JMn}\left|D^{2}_{0k}{}^{*}\alpha^{\mathrm{BF},(2,k)}\right|\Psi^{J'M'n'}\right\rangle\right.\\
&\quad\left. - \frac{1}{\sqrt{2}}\left\langle\Psi^{JMn}\left|\alpha^{\mathrm{BF},(0)}\right|\Psi^{J'M'n'}\right\rangle\right]\\
&= E^{Jn}\delta_{JJ'}\delta_{nn'}\delta_{MM'} - \delta_{MM'}\varepsilon(t)\sum_{k=-1}^{1}\left(\sum_{v,v'}\langle v\left|\mu^{\mathrm{BF},(1,k)}\right|v'\rangle\right.\\
&\quad\times\sum_{K,K'}C^{Jn^*}_{Kv}C^{J'n'}_{K'v'}(2J+1)^{\frac{1}{2}}(2J'+1)^{\frac{1}{2}}(-1)^{-k+M-K'}\\
&\quad\left.\times\begin{pmatrix} J & 1 & J'\\ M & 0 & -M\end{pmatrix}\begin{pmatrix} J & 1 & J'\\ K & -k & -K'\end{pmatrix}\right) - \delta_{MM'}\frac{\varepsilon^2(t)}{\sqrt{6}}\\
&\quad\times\sum_{k=-2}^{2}\left(\sum_{v,v'}\langle v\left|\alpha^{\mathrm{BF},(2,k)}\right|v'\rangle\sum_{K,K'}C^{Jn^*}_{Kv}C^{J'n'}_{K'v'}(2J+1)^{\frac{1}{2}}\right.\\
&\quad\left.\times(2J'+1)^{\frac{1}{2}}(-1)^{-k+M-K'}\begin{pmatrix} J & 2 & J'\\ M & 0 & -M\end{pmatrix}\begin{pmatrix} J & 2 & J'\\ K & -k & -K'\end{pmatrix}\right)\\
&\quad+\delta_{JJ'}\delta_{MM'}\frac{\varepsilon^2(t)}{\sqrt{12}}\sum_{v,v'}\sum_{K}C^{Jn^*}_{Kv}C^{J'n'}_{Kv'}\langle v\left|\alpha^{\mathrm{BF},(0)}\right|v'\rangle,
\end{aligned} \tag{7}$$

where E^{Jn} are the field-free eigenenergies of the system. If the bound rovibrational states $|\Psi^{JMn}\rangle$ and corresponding eigenvalues E^{Jn} are known, one only needs to evaluate the dipole $\langle v|\mu^{\mathrm{BF}}|v'\rangle$ and polarisability $\langle v|\alpha^{\mathrm{BF}}|v'\rangle$ matrix elements to construct the Hamiltonian matrix. It should be noted that the permanent dipole μ^{BF} and the polarisability α^{BF} are functions of the internal coordinates, i.e. $\langle v|\mu^{\mathrm{BF}}|v'\rangle \equiv \int\psi^*_v(Q_1,\ldots,Q_d)\mu^{BF}(Q_1,\ldots,Q_d)\times\psi_{v'}(Q_1,\ldots,Q_d)dQ_1,\ldots,dQ_d$ and $\langle v|\alpha^{\mathrm{BF}}|v'\rangle \equiv \int\psi^*_v(Q_1,\ldots,Q_d)\alpha^{BF}(Q_1,\ldots,Q_d)\psi_{v'}(Q_1,\ldots,Q_d)dQ_1,\ldots,dQ_d$.

While solving the TDSE in Equation (1), we monitor the time evolution of physical quantities by computing their expectation values with the rovibrational wavepacket at different times. This monitoring can be performed efficiently once the matrix representation of the respective physical quantities using the field-free basis states are computed beforehand. Based on the expansion of Equation (3), the matrixelements of a general function $f(Q_1,\ldots,Q_d)$ of the internal coordinates can be written as

$$\begin{aligned}
&\left\langle\Psi^{JMn}\left|f(Q_1,\ldots,Q_d)\right|\Psi^{J'M'n'}\right\rangle\\
&\quad = \delta_{JJ'}\delta_{MM'}\sum_{v,v'}\sum_{K}C^{Jn^*}_{Kv}C^{J'n'}_{Kv'}\langle v\left|f(Q_1,\ldots,Q_d)\right|v'\rangle.
\end{aligned} \tag{8}$$

For monitoring the alignment with the help of the ϕ angle between the z-axes of the BF and LF coordinate frames, the matrix elements of $\cos^2\phi$ can be written as [18]

$$\left\langle \Psi^{JMn} \left| \cos^2\phi \right| \Psi^{J'M'n'} \right\rangle = \sum_{\upsilon} \sum_{KK'} C_{K\upsilon}^{Jn^*} C_{K'\upsilon}^{J'n'} \left[\frac{1}{3}\delta_{JJ'}\delta_{KK'}\delta_{MM'} + \frac{2}{3}(2J+1)^{\frac{1}{2}}(2J'+1)^{\frac{1}{2}}(-1)^{M'+K'} \times \begin{pmatrix} J & 2 & J' \\ M & 0 & -M' \end{pmatrix} \begin{pmatrix} J & 2 & J' \\ K & 0 & -K' \end{pmatrix} \right]. \quad (9)$$

2.2. Bound state calculations

Theoretical estimates of the rovibrational energies and transitions of H_2He^+ have already been made [19–21] for facilitating its detection in outer space. However, to the best of our knowledge, no attempt has been made to obtain all the bound rovibrational energies and eigenstates on the ground electonic state of H_2He^+ by using the accurate PES of De Fazio *et al.* [22] called MRCI8.

For computing the field-free, bound rovibrational eigenstates of H_2He^+ supported by the PES calculated by De Fazio *et al.* [22], the full-dimensional variational computations in Jacobi coordinates were performed using the D^{2}FOPI protocol and the program suite [23], while the C_{2v}(M) molecular symmetry [9] was kept as described in [24]. In the D^{2}FOPI program, the time-independent rovibrational Schrödinger equation for a triatomic molecule is solved by an iterative engensolver using a mixed discrete variable representation (DVR) [25] and finite basis represenation [25], representing the vibrational degrees of freedom in an orthogonal coordinate system, and symmetry adopted Wigner matrices as rotational basis functions.

3. Computational details

During the computation of the bound rovibrational states of H_2He^+, for each irreducible representation of the C_{2v}(M) molecular symmetry group, we employ in the calculations (1) a complete set of rotational basis functions whose size varies depending on the given value of the J rotational quantum number, (2) 20 potential optimised (PO) spherical DVR basis functions [23] along the R coordinate, (3) 60 PO spherical DVR basis functions along the r coordinate, and (4) 15 associated Legendre funcions along the θ coordinate. The coordinate ranges used in the present calculations were R/bohr $\in (0, 4)$ and r/bohr $\in (0, 15)$, and the nuclear masses $m_H = 1.00727647$ u and $m_{He} = 4.00234755$ u were employed.

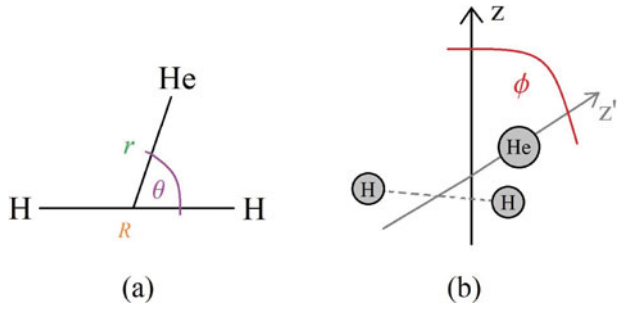

Figure 1. Pictorial representation of (a) the Jacobi coordinates [31] and (b) the angle between the laboratory-fixed and body-fixed z-axes. In terms of the Jacobi coordinates, the two linear equilibrium structures of H_2He^+ are located near the H − H distance of R = 2.09 bohr and the H_2^+ − He distance of r = 2.96 bohr, with θ = 0 or π [22].

With these parameters all rovibrational eigenenergies are converged to within 0.01 cm^{-1}, except for some of the highest lying states with very diffuse vibrational wavefunctions along the r coordinate, lying a few cm^{-1} below the dissociation energy. It is found that these high-lying diffuse vibrational states have a negligibly small population in the course of the simulation, and therefore, they do not influence the alignment dynamics of H_2He^+ investigated in this study.

The dipole moment μ^{BF} surface and the polarisability α^{BF}surface of H_2He^+ were constructed by interpolation on a uniform grid of 11,900 single-point calculations being carried out with Gaussian [26] on a CCSD/aug-cc-pVTZ level [27–29] level.

The matrix elements of the Hamiltonian of Equation (1) were computed according to Equation (7), using the bound rovibrational states previously determined. Due to the small size of the final Hamiltonian, time propagation can be carried out using the simple formula $\mathbf{\Psi}(t+dt) = e^{-\frac{i}{\hbar}\mathbf{H}(t)dt}\mathbf{\Psi}(t)$, where $e^{-\frac{i}{\hbar}\mathbf{H}(t)dt}$ is explicitly constructed by diagonalising $\mathbf{H}(t)$ at each timestep.

4. Results and discussion

4.1. Bound states

Based on the theoretical studies of De Fazio and colleagues [22,30], H_2He^+ has been known to take a linear equilibrium structure (see Figure 1) and its lowest spectroscopic dissociation energy is estimated to be only around 1780 cm^{-1} by $D_0 = D_e - E_{ZPVE}^{H_2He^+} + E_{ZPVE}^{H_2^+}$, with the dissociation energy, D_e = 2,740 cm^{-1}, the zero-point vibrational energy (ZPVE) of H_2He^+, $E_{ZPVE}^{H_2He^+}$ = 2110 cm^{-1}, and the ZPVE of H_2^+, $E_{ZPVE}^{H_2^+}$ = 1150 cm^{-1}.

Since H_2He^+ is so weakly bound, the ground-state PES supports only 16 bound vibrational states up to the first

dissociation limit, excluding the high-lying asymptotic vibrational states. For H_2^+, the first vibrational excitation energy is around 2200 cm^{-1}, which means that the H_2^+ moiety in H_2He^+ is in the vibrational ground state for all the bound H_2He^+ states. Indeed, no nodes can be observed along the R coordinate in the plots of the bound vibrational wavefunctions as shown in Figure 2. It can also be seen in panels (a) and (b) of Figure 2, that the lower energy eigenstates exhibit very narrow distributions along the θ coordinate around $\theta = 0$ or π, indicating a linear structure. Panel (d) of Figure 2 shows that He is delocalised to a large extent around the H_2^+ moiety in the vibrationally highly excited states and that the wavefunctions are very diffuse along the r coordinate.

The total number of bound rovibrational states is 430, excluding the high-lying diffuse vibrational states. The highest J rotational quantum number supporting bound states is $J = 20$. The eigenenergies of all computed rovibrational states are presented in Figure 3. By inspecting the wavefunction plots and the calculated expectation values of the projection K of the total angular momentum J along the BF z-axis, we find that the lower lying vibrational states and rovibrational states of H_2He^+ can be assigned with vibrational and rotational quantum numbers. We use the notation $(v_{\text{strech}}^{H_2} v_{\text{bend}}^{H_2-He} v_{\text{strech}}^{H_2-He})[JK]$, also employed in [21], where $v_{\text{strech}}^{H_2}$ and $v_{\text{strech}}^{H_2-He}$ are the quantum numbers for the streching motion along the R and r coordinates, respectively, $v_{\text{bend}}^{H_2-He}$ is the quantum number for the bending along θ, J is the total rotational quantum number and K is the projection of the rotational angular momentum onto the BF z-axis. Based on the assignments presented in Figure 3, it can be seen that there is a well-separated group of eigenstates with the quantum numbers $(0\,0\,0)[J\,0]$, corresponding to a non-vibrating linear rotor with purely rotational excitations. On the other hand, vibrational and rotational excitation energies can be on the same magnitude even for low-lying levels, as can be seen, for example, in the vibrationally excited $(0\,0\,1)[0\,0]$ state and in the rotationally excited $(0\,0\,0)[1\,1]$ state shown in Figure 3. Indeed, except for the group of $(0\,0\,0)[J\,0]$ states discussed above, the rigid rotor approximation could not be applied due to the strong coupling between the rotational and vibrational degrees of freedom.

4.2. Alignment dynamics

By adopting the theoretical methods detailed in Section 2, we simulate the laser-induced rovibrational dynamics of H_2He^+ under various laser conditons starting from the rovibratioal ground state. Figure 4 presents the temporal variation of selected physical quantities, calculated when H_2He^+ is excited by a linearly polarised Gaussian laser pulse with the parameters, $\lambda = 800$ nm, $I = 10^{13}$ W cm^{-2}, and half-width = 6.7 ps. Figure 4 demonstrates the example of adiabatic alignment. As shown in this figure, when a laser pulse is long enough with respect to the rotational timescale of the system, H_2He^+ gradually aligns along the laser polarisation axis starting from an isotropic distribution with $\langle\cos^2(\phi)\rangle = 1/3$, and, as the laser field decreases and disappears, the distribution returns to be isotropic in accordance with the adiabatic theorem [32]. No significant structural deformation is identified during this process. Indeed, the H–H and H–He bond lengths and the H-H–He bond angle exhibit negligiblly small changes in Figure 4 as a function of time. It can be concluded that under these laser conditions the adiabatic alignment is achieved by the creation of a purely rotational wavepacket.

In Figure 5 the non-adiabatic alignment dynamics of H_2He^+ is seen when H_2He^+ is exposed to a linearly polarised Gaussian laser pulse ($\lambda = 800$ nm, $I = 2 \times 10^{13}$ W cm^{-2}, and half-width = 330 fs). A full revival time of 4 ps can be seen in Figure 5. As has been seen in Figure 4, no significant laser-induced structural change is seen in Figure 5, indicating that a purely rotationally excited wavepacket is created. This pure rotational excitation of the wavepacket can be confirmed by the populations in the different rovibrational eigenstates forming the wavepacket created after the interaction with the laser field as shown in panel (a) of Figure 6, in which the rovibrational states with a non-negligible population are all labelled with the quantum numbers $(0\,0\,0)[J\,0]$. It is true that the rotational level energies are shifted slightly by the centrifugal distortion and a revival time could not be defined in a rigorous manner, but a full revival time of 4 ps can be identifed in Figure 5, showing that the centrifugal distortion is sufficiently small in this case.

When H_2He^+ is exposed to a linearly polarised Gaussian laser pulse ($\lambda = 25{,}000$ nm, $I = 10^{12}$ Wcm^{-2}, and half-width = 240 fs), the non-adiabatic alignment dynamics of H_2He^+ becomes as shown in Figure 7. It is clear from Figure 7 that the molecule undergoes substantial structural change when the laser wavelength is chosen to be closer to resonance with vibrational excitation. Due to the superposition of several vibrational eigenstates in the wavepacket as seen in panel (b) of Figure 6, the expectation value of geometrical parameters changes as a function of time. This leads to the temporal change of the rotational constants as well, which in turn leads to very complex alignment dynamics with no evident revival time. As can be seen in Figure 7, the expectation value of R shrinks while the expectation value of r increases by the interaction with the laser field. This can be understood

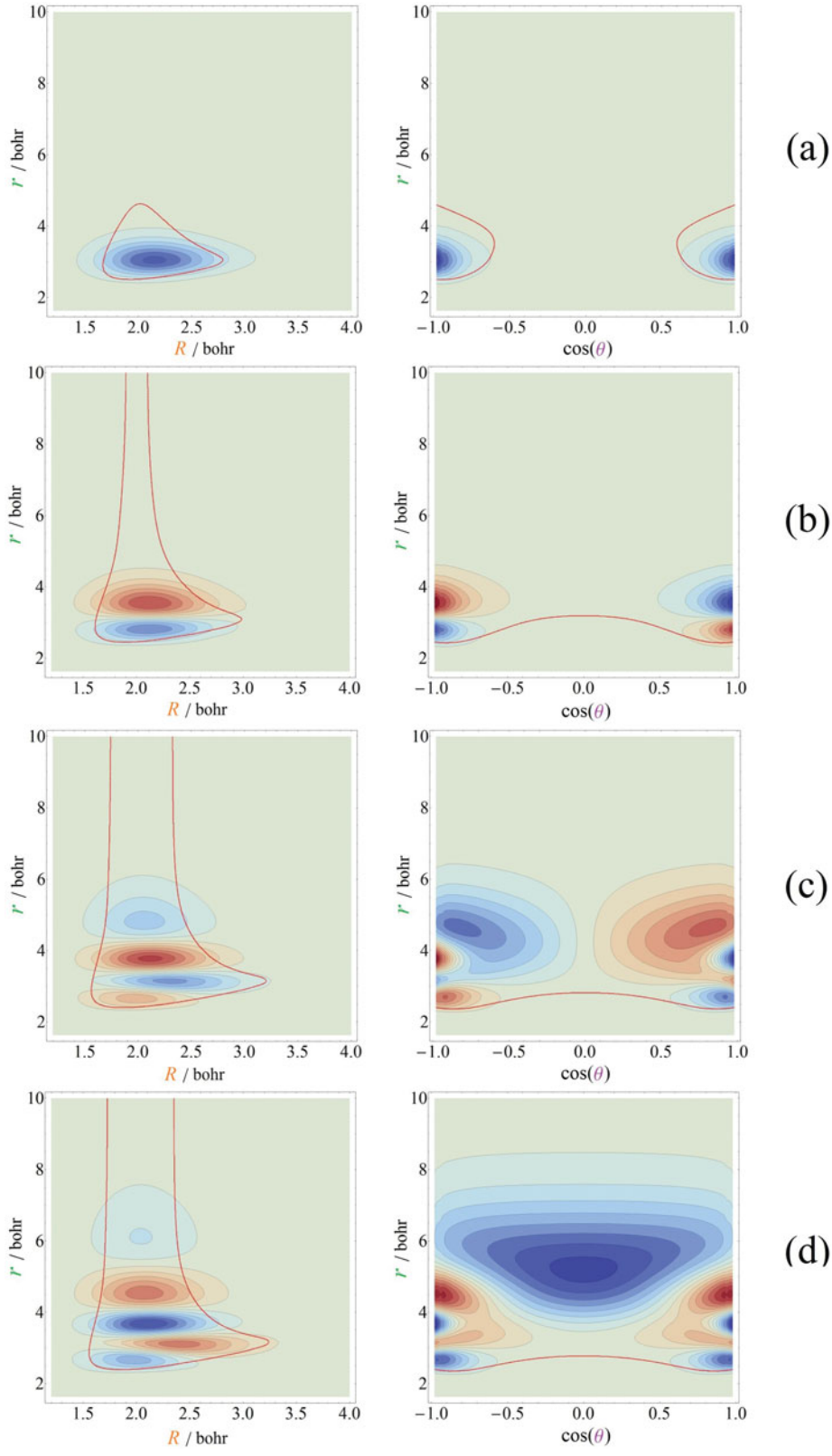

Figure 2. Contour plots of the wave functions of selected vibrational states of H_2He^+. The wavefunctions correspond to (a) the ground vibrational state with energy 2107.00 cm^{-1}, (b) the 3rd excited vibrational state with energy 2840.77 cm^{-1}, (c) the 9th excited vibrational state with energy 3653.34 cm^{-1}, and (d) the 12th excited vibrational state with energy 3789.05 cm^{-1}. A thin curve in each frame represents the energy of the vibrational eigenstate, that is, the border of the classically allowed region for molecular vibration.

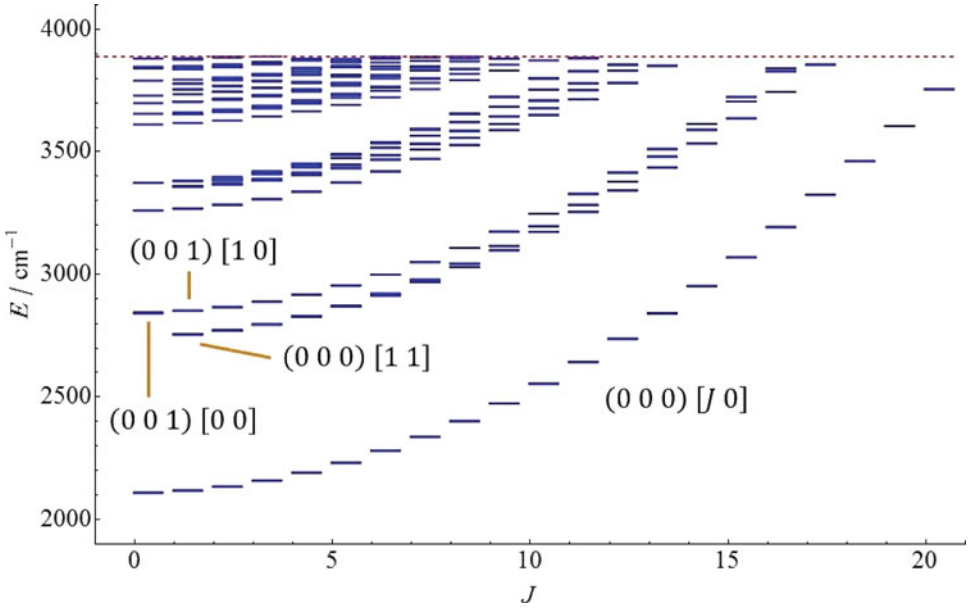

Figure 3. Rovibrational energy levels of H_2He^+ suppported by the PES of De Fazio *et al*. [22], as function of the *J* total rotational quantum number. The dashed line marks the first dissociation energy. See text for the definitions of the quantum numbers.

by comparing the ground and excited vibrational states of the H_2He^+ molecule, shown in panels (a) and (b–d) of Figure 2, respectively. In the case of vibrationally excited states, which are being populated during the laser–matter interaction, the wavefunction expands along the *r* coordinate. With increasing *r*, however, as the He gets farther away from the H_2^+ moiety, $V(R)$ becomes deeper, leading to a wavefunction with a narrower distribution along *R* and shorter *R* expectation value.

Finally, in Figure 8, we compare the results of the simulations obtained with the full-dimensional approach and those obtained within the rigid rotor approximation. The upper panel of Figure 8 shows the alignment dynamics of H_2He^+ when it is irradiated with 800-nm-wavelength light pulse ($I = 5 \times 10^{13}$ W cm^{-2}, half-width = 165 fs). Since only the rovibrational states characterised by the quantum numbers (0 0 0)[*J* 0] are populated in this case, the full-dimensional and rigid rotor simulations show excellent agreement up to a few picoseconds

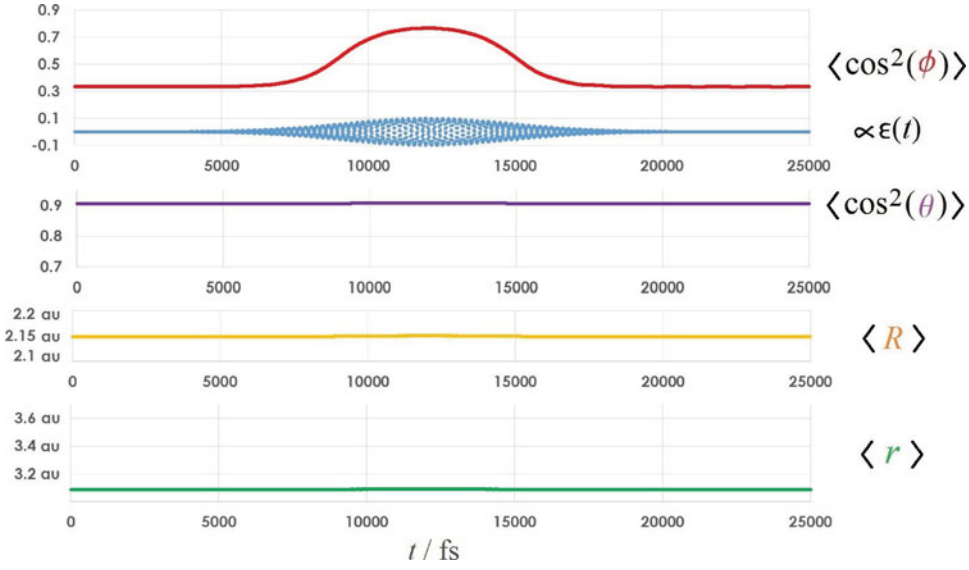

Figure 4. Temporal change in the expectation values of the structural parameters and the alignment of H_2He^+ when it is exposed to a laser field with the parameters $\lambda = 800$ nm, $I = 10^{13}$ W cm^{-2}, and half-width = 6.7 ps.

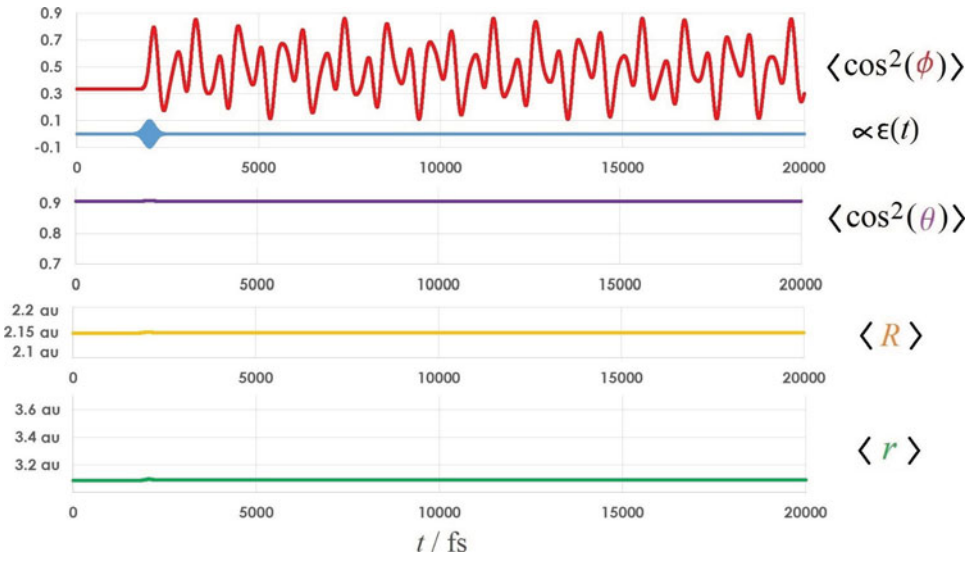

Figure 5. Temporal change of the expectation values of structural parameters and the alignment of H_2He^+ when exposed to a laser field with parameters $\lambda = 800$ nm, $I = 2 \times 10^{13}$ W cm^{-2}, and half-width = 330 fs.

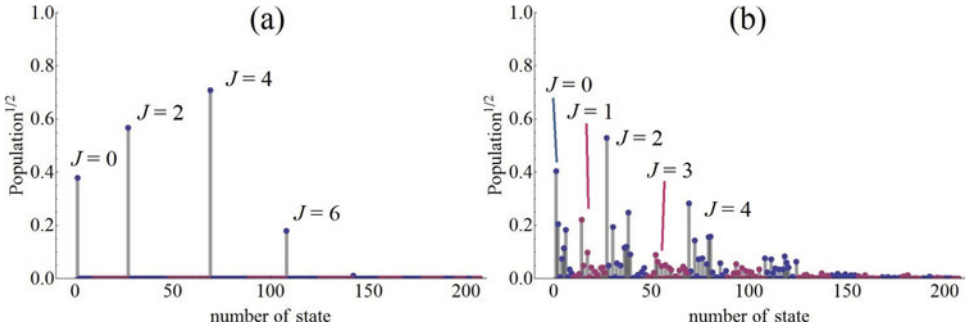

Figure 6. Relative populations in the different rovibrational states in the wavepacket of H_2He^+ induced by a laser pulse with parameters (a) $\lambda = 800$ nm, $I = 2 \times 10^{13}$ W cm^{-2}, half-width = 330 fs, and (b) $\lambda = 25{,}000$ nm, $I = 10^{12}$ W cm^{-2}, half-width = 240 fs. We show the square roots of the populations in order to see clearly the populations in the rotational levels populated only to a small extent.

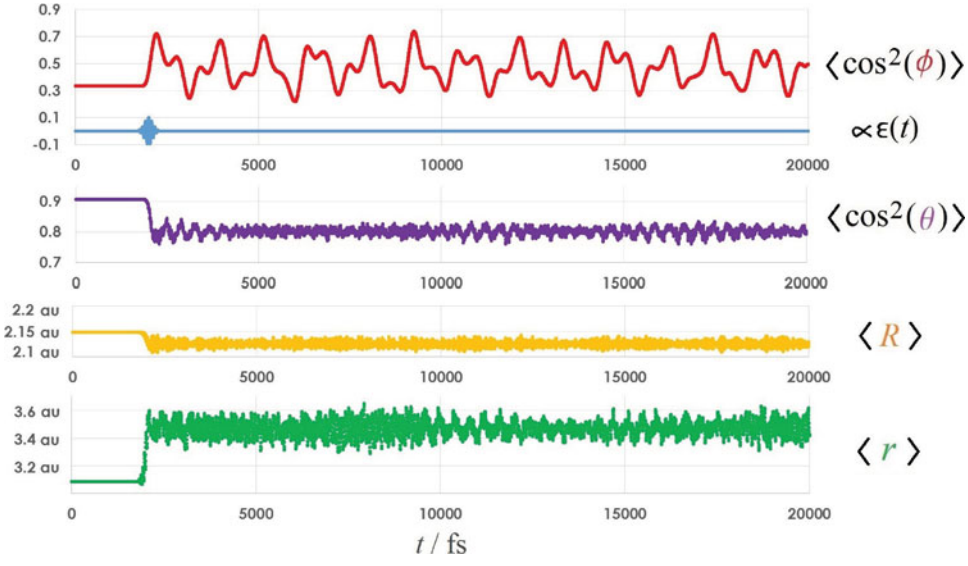

Figure 7. Temporal change of the expectation values of structural parameters and the alignment of H_2He^+ when exposed to a laser field with parameters $\lambda = 25{,}000$ nm, $I = 10^{12}$ W cm^{-2}, and half-width = 240 fs.

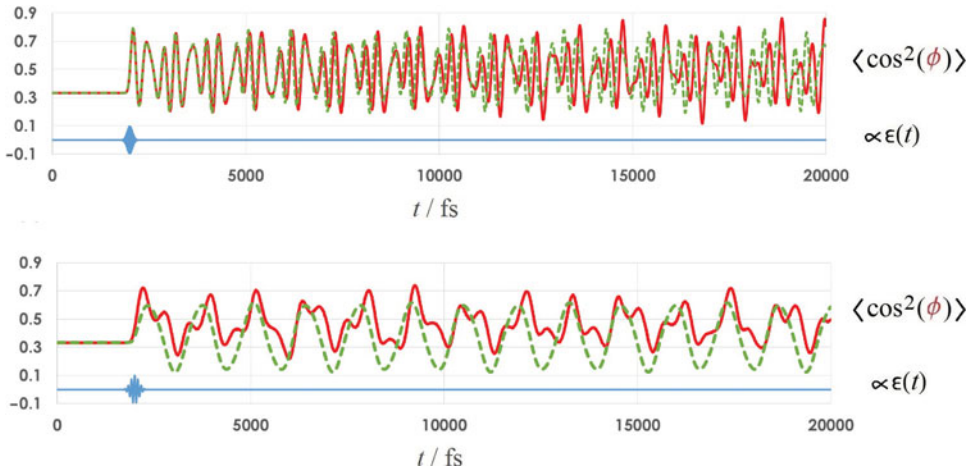

Figure 8. Temporal change of the expectation values of the alignment of H_2He^+ computed with the (dashed curves) rigid rotor approximation and (solid curves) the full-dimensional approach of this work. The upper panel was obtained with the laser parameters set to $\lambda = 800$ nm, $I = 5 \times 10^{13}$ W cm^{-2}, half-width = 165 fs, while the lower panel was obtained with the laser parameters $\lambda = 25{,}000$ nm, $I = 10^{12}$ W cm^{-2}, half-width = 240 fs.

after the interaction with the laser pulse. However, due to centrifugal distortion, the rotational energies in the full-dimensional approach are shifted to lower values, which eventually on a longer time scale leads to large differences in the relative phases of the eigenstates in the wavepacket. Therefore, the rotational revivals become shifted in time as well, and the results of the simulations in the two cases deviate from each other. The lower panel of Figure 8 presents the case when H_2He^+ is irradiated by a 25,000-nm-wavelength laser pulse ($I = 10^{12}$ W cm^{-2}, and half-width = 240 fs). In this case, rotational as well as vibrational excitation occurs in the full-dimensional model; therefore, the rigid rotor model is no longer a good approximation.

5. Summary and conclusion

A simple and general theoretical framework was presented, which can be utilised to simulate the laser-induced alignment dynamics of non-rigid polyatomic molecules. The approach is based on solving the TDSE by expanding the laser-induced wavepacket with the field-free rovibrational eigenstates of the system. If the field-free eigenstates are obtained with very high accuracy, the numerically exact solutions of the TDSE can be obtained. On the other hand, if the field-free eigenstates are obtained with approximate, computationally less demanding methods, the solution of the TDSE will be approximate as well.

As a numerical example, the laser-induced alignment dynamics of weakly bound H_2He^+ was investigated. By the full-dimensional computations on the nuclear motion with high accuracy, the bound rovibrational eigenstates of H_2He^+ were computed and used as basis functions for describing the laser-induced alignment dynamics of the molecule.

Our findings are as follows:

(1) H_2He^+ has around 430 bound rovibrational states, 34 of which exhibit a near linear structure ($\langle\cos^2(\theta)\rangle$ is larger than 0.95).
(2) In all bound states of H_2He^+, the H_2^+ moiety is in its ground vibrational state.
(3) Except a group of purely rotationally excited eigenstates, which can be characterised with the quantum numbers (0 0 0)[J 0], the rovibrational states of H_2He^+ are subject to strong rovibrational couplings, as represented by almost the same excitation energies in the vibrational and rotational degrees of freedom.
(4) When H_2He^+ is exposed to a long laser pulse ($\lambda = 800$ nm, half-width = 6.7 ps, $I = 10^{13}$ W cm^{-2}), the molecule undergoes adiabatic alignment during which a purely rotational wavepacket is formed. By the time when the laser field subsides, the ensemble of the molecules returns adiabatically to the randomly oriented distribution.
(5) If a much shorter laser pulse ($\lambda = 800$ nm, half-width = 330 fs, $I = 2 \times 10^{13}$ W cm^{-2}) is adopted, which is off resonance with vibrational excitations, a purely rotational wavepacket is created and H_2He^+ shows field-free alignment dynamics with a full revival time of around 4 ps.
(6) By changing the wavelength of the laser to be closer to resonance with the first vibrational excitation energy ($\lambda = 25{,}000$ nm, half-width =

240 fs, $I = 10^{12}$ W cm^{-2}), H_2He^+ undergoes significant structural changes, i.e. the distance between the He and the H_2^+ moiety increases while the H–H bond shortens. The expectation value $\langle\cos^2(\theta)\rangle$ also decreases, and all structural parameters exhibit rapid fluctuation in time. The temporal change in the geometrical structure of H_2He^+ leads to the temporal variation in the rotational constants, and consequently, the non-adiabatic rotational dynamics of H_2He^+ ends up with showing no evident revival time.

(7) When H_2He^+ is irradiated with a 800-nm-wavelength light pulse ($I = 5 \times 10^{13}$ W cm^{-2}, half-width = 165 fs), the rigid rotor approximation shows excellent agreement with the full-dimensional calculations up to a few picoseconds, but due to centrifugal distortion starts exhibiting the deviation as time goes on.

(8) When H_2He^+ is irradiated with a 25,000-nm-wavelength laser pulse ($I = 10^{12}$ W cm^{-2}, and half-width = 240 fs), which induces rotational as well as vibrational excitation, the rigid rotor approximation can no longer be applicable for obtaining accurate results on the alignment dynamics, and consequently, the full-dimensional approach is required.

The theoretical framework proposed and demonstrated in the present study on laser-induced alignment of H_2He^+ can be applied to a wide range of molecules as long as their accurate rovibrational eigenstates necessary for describing the laser-induced dynamics of the system are generated.

Disclosure statement

No potential conflict of interest was reported by the authors.

Funding

The work described received support from the Grant-in-Aid (Tokubetsu Kenkyuin Shorei-hi) scientific research fund of Japan Society for the Promotion of Science (JSPS) (project number 26-04333); the JSPS KAKENHI [grant number 15H05696].

References

[1] H. Stapefeldt and T. Seideman, Rev. Mod. Phys. **75**, 543 (2003).
[2] Y. Ohshima and H. Hasegawa, Int. Rev. Phys. Chem. **29**, 619 (2010).
[3] M. Lemeshko, R.V. Krems, J.M. Doyle and S. Kais, Mol. Phys. **111**, 1648 (2013).
[4] O. Faucher, B. Lavorel, E. Hertz and F. Chaussard, *Progress in Ultrafast Intense Laser Science* (Springer-Verlag, Berlin Heidelberg, 2011), Vol. **VII**, Chap. 4.
[5] H. Hasegawa and Y. Ohshima, *Progress in Ultrafast Intense Laser Science* (Springer International Publishing, Switzerland, 2015), Vol. **XII**, Chap. 3.
[6] J. Floß, T, Grohmann, M. Leibscher and T. Seideman, J. Chem. Phys. **136**, 084309 (2012).
[7] C.M. Dion, A. Keller, O. Atabek and A.D. Bandrauk, Phys. Rev. A **59**, 1382 (1999).
[8] C.C. Shu and N.E. Henriksen, J. Chem. Phys. **142**, 221101 (2015).
[9] P.R. Bunker and P. Jensen, *Molecular Symmetry and Spectroscopy* (NRC Research Press, Ottawa, 1998).
[10] A.G. Császár, C. Fábri, T. Szidarovszky, E. Mátyus, T. Furtenbacher and G. Czakó, Phys. Chem. Chem. Phys. **14**, 1085 (2012); and references therein.
[11] J. Tennyson, J. Chem. Phys. **145**, 120901 (2016); and references therein.
[12] S.N. Yurchenko, W. Thiel and P. Jensen, Mol. Spectrosc. **245**, 126 (2007).
[13] J.M. Bowman, S. Carter and X.-C. Huang, Int. Rev. Phys. Chem. **22**, 533 (2003).
[14] R.J. Barber, J. Tennyson, G.J. Harris and R.N. Tolchenov, Mon. Not. Roy. Astron. Soc. **368**, 1087 (2006).
[15] C. Fábri, E. Mátyus and A.G. Császár, J. Chem. Phys. **134**, 074105 (2011).
[16] V. Barone, M. Biczysko and J. Blonio, Phys. Chem. Chem. Phys. **16**, 1759 (2014).
[17] R.N. Zare, *Angular Momentum* (Wiley, New York, 1988).
[18] V. Makhija, X. Ren and V. Kumarappan, Phys. Rev. A **85**, 033425 (2012).
[19] M. Juřek, V. Špirko and W.P. Kraemer, J. Mol. Sprectrosc. **182**, 364 (1997).
[20] M. Šindelka, V. Špirko and W.P. Kraemer, Theor. Chem. Acc. **110**, 170 (2003).
[21] J. Tennyson and S. Miller, J. Chem. Phys. **87**, 6648 (1987).
[22] D. De Fazio, M. de Castro-Vitores, A. Aguado, V. Aquilanti and S. Cavalli, J. Chem. Phys. **137**, 244306 (2012).
[23] T. Szidarovszky, A.G. Császár and G. Czakó, Phys. Chem. Chem. Phys. **12**, 8373 (2010).
[24] T. Szidarovszky and A.G. Császár, Mol. Phys. (Martin Quack Special Issue) **111**, 2131 (2013).
[25] J.C. Light and T. Carrington Jr., Adv. Chem. Phys. **114**, 263 (2000).
[26] M.J. Frisch, G.W. Trucks, H.B. Schlegel, G.E. Scuseria, M.A. Robb, J.R. Cheeseman, G. Scalmani, V. Barone, B. Mennucci, G.A. Petersson, H. Nakatsuji, M. Caricato, X. Li, H.P. Hratchian, A.F. Izmaylov, J. Bloino, G. Zheng, J.L. Sonnenberg, M. Hada, M. Ehara, K. Toyota, R. Fukuda, J. Hasegawa, M. Ishida, T. Nakajima, Y. Honda, O. Kitao, H. Nakai, T. Vreven, J.A. Montgomery, Jr., J.E. Peralta, F. Ogliaro, M. Bearpark, J.J. Heyd, E. Brothers, K.N. Kudin, V.N. Staroverov, R. Kobayashi, J. Normand, K. Raghavachari, A. Rendell, J.C. Burant, S.S. Iyengar, J. Tomasi, M. Cossi, N. Rega, J.M. Millam, M. Klene, J.E. Knox, J.B. Cross, V. Bakken, C. Adamo, J. Jaramillo, R. Gomperts, R.E. Stratmann, O. Yazyev, A.J. Austin, R. Cammi, C. Pomelli, J.W. Ochterski, R.L. Martin, K.

Morokuma, V.G. Zakrzewski, G.A. Voth, P. Salvador, J.J. Dannenberg, S. Dapprich, A.D. Daniels, Ö. Farkas, J.B. Foresman, J.V. Ortiz, J. Cioslowski and D.J. Fox, *Gaussian, Inc.* (Gaussian, Inc., Wallingford, CT, 2009).

[27] R.J. Bartlett, C.E. Dykstra and J. Paldus, *Advanced Theories and Computational Approaches to the Electronic Structure of Molecules* (Reidel, Dordrecht, 1984).

[28] T.H. Dunning Jr., J. Chem. Phys. **90**, 1007 (1989).

[29] R.A. Kendall, T.H. Dunning Jr. and R.J. Harrison, J. Chem. Phys. **96**, 6796 (1992).

[30] P. Palmieri, C. Puzzarini, V. Aquilanti, G. Capecchi, S. Cavalli, D. DeFazio, A. Aguilar, X. Giménez and J.M. Lucas, Mol. Phys. **98**, 1835 (2000).

[31] C.G.J. Jacobi and Cr. Hebd, Acad. Sci. **15**, 236 (1842).

[32] M. Born and V.A. Fock, Z. Physik **51**, 165 (1928).